

1 **Spectral properties of whistler-mode waves in the**
2 **vicinity of the Moon: A statistical study with**
3 **ARTEMIS**

4 **W. Sawaguchi¹, Y. Harada¹, S. Kurita², and S. Nakamura³**

5 ¹Department of Geophysics, Graduate School of Science, Kyoto University, Kyoto, Japan.

6 ²Research Institute for Sustainable Humanosphere, Kyoto University, Uji, Japan.

7 ³Institute for Space-Earth Environmental Research, Nagoya University, Nagoya, Japan.

8 **Key Points:**

- 9 • We present a statistical study on Moon-related whistler-mode waves classified into
10 4 types of spectral shapes using ARTEMIS data
- 11 • Banded waves are extremely rare, suggesting that two band structure formation
12 is ineffective around the Moon
- 13 • Whistler-mode wave spectra are highly variable resulting from spatial and tem-
14 poral variability of the lunar plasma environment

Corresponding author: Wataru Sawaguchi, sawag@kugi.kyoto-u.ac.jp

15 **Abstract**

16 We present statistical analyses of whistler-mode waves observed by Acceleration, Recon-
 17 nection, Turbulence and Electrodynamics of the Moon’s Interaction with the Sun (ARTEMIS).
 18 Although some observations showed rising tone elements of the lunar whistler-mode waves
 19 similar to the terrestrial chorus emissions, it remains unknown whether a banded struc-
 20 ture typically seen in chorus is common to the lunar waves. In this study, we automat-
 21 ically detected whistler-mode waves from 9 years of ARTEMIS data and classified them
 22 into four types of spectral shapes: lower band only, upper band only, banded, and no-
 23 gap. We first show that magnetic connection to the lunar surface is a dominant factor
 24 in the wave generation; the occurrence rate of whistler mode waves is more than 10 times
 25 larger on magnetic field lines connected to the Moon than on unconnected field lines. Then
 26 we compared the field line connected events according to the position of the Moon and
 27 the condition of the field-line foot point (day/night and existence of lunar magnetic anoma-
 28 lies). The results show that (i) almost no banded event is observed in any circumstances,
 29 suggesting that generation mechanisms for the two band structure on the terrestrial cho-
 30 rus are largely ineffective around the Moon, and (ii) the wave occurrence rate depends
 31 on the foot point conditions, presumably affected by electrostatic/magnetic reflections
 32 deforming the velocity distribution of the resonant electrons. Thus, our results provide
 33 implications for the two band structure formation and new insights to fundamental pro-
 34 cesses of the Moon-plasma interaction.

35 **1 Introduction**

36 Whistler-mode waves in space are generally electromagnetic waves excited at fre-
 37 quencies below the electron cyclotron frequency (f_{ce}). Here, $f_{ce} = eB/2\pi m$, where e
 38 and m are the absolute value of the electron charge and mass, respectively, and B is the
 39 background magnetic field strength. In the linear growth theory in cold plasmas (Kennel
 40 & Petschek, 1966), the excitation efficiency of whistler-mode waves depends on the tem-
 41 perature anisotropy and the population of resonant electrons. The excitation needs a per-
 42 pendicular temperature higher than a parallel temperature and abundant hot electrons.
 43 The temperature anisotropy originates, for example, from perpendicular heating of elec-
 44 trons injected from the magnetotail during substorms. A well-known example of whistler-
 45 mode waves is chorus emissions that have been extensively studied in the terrestrial in-
 46 ner magnetosphere (e.g. Burtis & Helliwell, 1969, 1976; Tsurutani & Smith, 1974) and

47 also identified in the magnetospheres of Jupiter (Coroniti et al., 1980; Scarf et al., 1981;
 48 Menietti, Horne, et al., 2008), Saturn (Hospodarsky et al., 2008; Menietti, Santolik, et
 49 al., 2008), and Mars (Harada et al., 2016). In the terrestrial magnetosphere, chorus emis-
 50 sions are known to be excited near the magnetic equator, where resonant electrons tend
 51 to be abundant because the magnetic field strength is minimal and therefore the reso-
 52 nant velocity is small. Chorus emissions have been implicated in diffuse auroras and the
 53 outer radiation belt through electron acceleration (Horne et al., 2005; Thorne et al., 2013).
 54 A characteristic feature of chorus emissions is rising (or falling) tone elements, in which
 55 the frequency rises (or falls) in a short period less than 1 second. The generation of the
 56 rising tone can be explained by the nonlinear growth theory, which takes into account
 57 the second-order terms of cyclotron resonance (Omura et al., 2008; Omura, 2021). Sim-
 58 ulations (Omura et al., 2008; Katoh & Omura, 2011) reproduce the rising tone, and also
 59 the time evolution of the rising frequency and the growing amplitude in simulations and
 60 observations show a good agreement with the theory (Cully et al., 2011; Kurita et al.,
 61 2012).

62 Another typical feature of chorus emissions is a two-band structure in the spectrum
 63 with an intensity gap around $0.5 f_{ce}$, making a separation into two frequency bands, the
 64 lower band and the upper band (Burtis & Helliwell, 1969, 1976; Tsurutani & Smith, 1974).
 65 Teng et al. (2019) have statistically demonstrated the common presence of two-band struc-
 66 ture in the terrestrial whistler-mode waves, showing the ratio of two-band to no-gap waves
 67 is 3:1 in the observations of Van Allen probes. Similarly, Gao et al. (2019) found a 2:1
 68 ratio of multi-band and no-gap waves in the Time History of Events and Macroscale In-
 69 teractions during Substorms (THEMIS) magnetic field waveform data from a statisti-
 70 cal analysis using different criteria. Despite decades of research, the formation mecha-
 71 nisms of the two-band structure remain a long-standing question. One of the leading hy-
 72 potheses is that Landau damping creates an intensity gap at $0.5 f_{ce}$ (Tsurutani & Smith,
 73 1974; Omura et al., 2009). They have proposed that a rising tone is first excited as a con-
 74 tinuous element extending over both bands and propagates parallel to the field line. Dur-
 75 ing the propagation, the waves gradually becomes oblique and exhibit an electrostatic
 76 component due to the curvature of the field line at the off-equator, which causes the Lan-
 77 dau resonance. In some circumstances (i.e. electrons bouncing between magnetic mir-
 78 rors), $0.5 f_{ce}$ waves can be efficiently Landau-damped by co-streaming electrons in cy-
 79 clotron resonances with counter-streaming waves, because the cyclotron resonance ve-

80 locity equals in the magnitude but opposite to the wave phase velocity (Tsurutani & Smith,
 81 1974). The propagation of waves widens the gap as an off-equatorial f_{ce} increases from
 82 the equatorial f_{ce} with the increasing magnetic field strength. Gao et al. (2016) proposed
 83 another mechanism called the lower band cascade mechanism, in which upper band waves
 84 are excited as a harmonic structure through the coupling of a lower band electromag-
 85 netic wave with an electrostatic density mode wave of approximately equal frequency.
 86 In another study, Fu et al. (2014) argued from PIC simulation results that the lower and
 87 upper bands can be generated by two anisotropic electron components with different tem-
 88 peratures, and that a gap is formed between them as a natural consequence. Each of these
 89 theories alone cannot fully explain observed results as follows. Habagishi et al. (2014)
 90 supported the Landau damping scenario by showing a clear correspondence of higher and
 91 lower frequency edges of the gap with the local $0.5 f_{ce}$ and the equatorial $0.5 f_{ce}$. On
 92 the other hand, smaller occurrence rates of no-gap events near the magnetic equator are
 93 contrary to the consequences from the Landau scenario (Teng et al., 2019; Gao et al.,
 94 2019). Gao et al. (2019) have suggested that power gaps could be a result of a combi-
 95 nation of several different mechanisms, based on two types of banded chorus different
 96 in the intensity and electrostatic nature of upper band waves.

97 Unlike the Earth, the Moon is an airless body with no global intrinsic magnetic field.
 98 As the Moon orbits around the Earth, it passes through the solar wind, terrestrial mag-
 99 netosheath, and terrestrial magnetotail. These regions are characterized by very differ-
 100 ent plasma parameters, so the external plasma surrounding the Moon is greatly variable
 101 (e.g. Harada & Halekas, 2016). In addition, the lunar surface is known to be electrostat-
 102 ically charged in response to the input and output of charges from and to the ambient
 103 plasma (Whipple, 1981). The lunar surface charging is determined by the balance be-
 104 tween the charged particle flux absorbed by the lunar surface and that emitted from the
 105 surface. On the sunlit surface, the dominant current is a downward current toward the
 106 lunar surface provided by photoelectrons emission, which results in a positive charge and
 107 positive potential on the day side. On the night side of the Moon, the ambient electron
 108 current prevails because of a higher thermal speed of electrons than ions, and thus the
 109 accumulated negative charge results in a negative electrostatic potential.

110 Recent observations revealed the presence of whistler-mode waves excited near the
 111 Moon (Halekas, Poppe, Farrell, et al., 2012; Harada et al., 2014, 2015). Moon-related
 112 whistler-mode waves are excited by upward traveling electrons along field lines connected

113 to the Moon. The free energy source for the wave excitation is provided by an effective
114 temperature anisotropy in upward electrons resulting from the anisotropic reflection; in-
115 cident electrons with larger pitch angles are reflected by lunar crustal magnetic fields while
116 smaller pitch angle electrons are absorbed at the lunar surface. Harada et al. (2014) found
117 that the intensity of whistler-mode waves is generally weakened on field lines connected
118 to strong magnetic anomalies, which could be attributable to the reduction of the effec-
119 tive temperature anisotropy due to stronger magnetic magnetic reflection leading to more
120 isotropic distributions of upward traveling electrons. Furthermore, Sawaguchi et al. (2021)
121 reported that lunar whistler-mode waves can form chorus-like rising tone elements con-
122 sistent with the nonlinear growth theory of Omura et al. (2008) in the relationship be-
123 tween frequency sweep rates and the amplitudes. The presence of rising tone elements
124 at the Moon suggests that a common physical process can operate for whistler-mode waves
125 both at the Moon and in the terrestrial inner magnetosphere, and that the lunar envi-
126 ronment provides a useful test case for chorus research. However, another typical fea-
127 ture of chorus emissions, the two-band structure, has not been investigated and it remains
128 unclear whether it exists around the Moon or not.

129 In this study, we conduct a statistical study of spectral properties of whistler-mode
130 waves in the vicinity of the Moon by utilizing Acceleration, Reconnection, Turbulence,
131 and Electrodynamics of the Moon’s Interaction with the Sun (ARTEMIS) observations.
132 Following the methodology of Teng et al. (2019) for the terrestrial inner magnetosphere,
133 we classify spectral shapes of the Moon-related whistler-mode waves into four categories,
134 including the two-band structure, and statistically investigate their occurrence rates. In
135 addition, we also investigate variations of the spectral properties in different plasma en-
136 vironments of the Moon. These investigations could provide further insights into the uni-
137 versality of the proposed generation mechanisms of the two-band chorus emissions and
138 into the temporally and spatially variable plasma environment around the Moon.

139 **2 Data and methodology**

140 We analyze data obtained by the ARTEMIS mission (Angelopoulos, 2011) from July
141 2011 to June 2020. We utilize onboard FFT spectra of wave magnetic field from Search
142 Coil Magnetometer (SCM; Roux et al., 2008) and background magnetic field vector data
143 from Fluxgate Magnetometer (Auster et al., 2008).

144 We process the onboard FFT data in the following manner. We first exclude in-
 145 tense broadband noise, which is likely to be caused by artificial contamination such as
 146 spike noises, from statistics by rejecting a spectrum if the power given by integrating the
 147 power spectral density over frequencies above $1f_{ce}$ exceeds 10^{-5} nT². Then we perform
 148 automatic identification of whistler-mode waves and classification of them according to
 149 their spectral shapes by adapting the methodology of Teng et al. (2019). For a given spec-
 150 trum as a function of the wave frequency f , we identify a whistler-mode wave event if
 151 the maximum power spectral density in a frequency range of $0.1 < f/f_{ce} < 0.8$ is larger
 152 than a threshold value of $p_{th} = 10^{-6}$ nT²/Hz. Note that the threshold value is set two
 153 orders of magnitude higher than Teng et al. (2019) to take into account the higher noise
 154 floor of the SCM onboard spectra in the corresponding frequency range than that of burst
 155 mode wave data by Van Allen probes used in Teng et al. (2019). Also, the frequency range
 156 is restricted to above 10 Hz because the data below 10 Hz contain a considerable amount
 157 of noises. In addition, if the aforementioned maximum power does not form a peak with
 158 a positive spectral slope in the frequency range of $0.1 < f/f_{ce} < 0.8$ and $f > 10$ Hz,
 159 the data point is treated as “no wave” to avoid misdetection of a part of other lower fre-
 160 quency waves.

161 Next, the identified whistler-mode wave events are classified into four categories
 162 of spectral shapes: lower band only, upper band only, no-gap, and banded waves. Fig-
 163 ure 1 shows examples of the spectrum of the four types of events. The gap frequency f_{gapmin}
 164 is defined as the frequency at which the power of the wave takes the minimum value p_{gapmin}
 165 within a frequency range of $0.45 < f/f_{ce} < 0.55$. Then the power of lower band and
 166 upper band, p_L and p_U , are defined as the maximum values within $0.1f_{ce} < f < f_{gapmin}$
 167 and $f_{gapmin} < f < 0.8f_{ce}$, respectively. If $p_L > p_{th}$ and $p_U < p_{th}$, then the waves are
 168 identified as lower band only waves. The case of $p_L < p_{th}$ and $p_U > p_{th}$ is defined as
 169 upper band only waves. In cases that both p_L and p_U are higher than p_{th} , those events
 170 with p_L and p_U both of which are higher than $10^{1.5}p_{gapmin}$ are defined as banded waves,
 171 and the rest are considered as no-gap waves. We also tested the algorithm using THEMIS
 172 data obtained in the terrestrial inner magnetosphere and validated that the algorithm
 173 is capable of discriminating between the banded and no-gap waves with onboard FFT
 174 spectra of THEMIS-ARTEMIS/SCM (see Supporting Information for details).

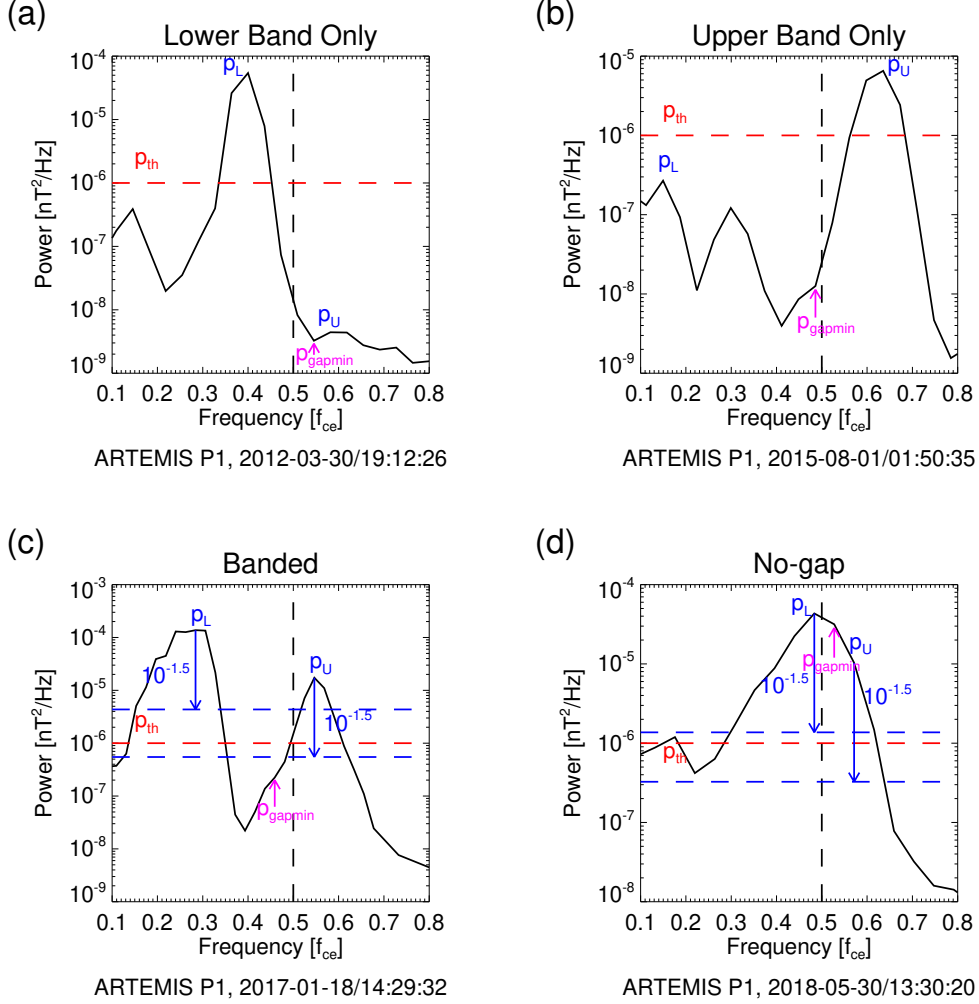


Figure 1. Examples of spectra of events observed by ARTEMIS SCM. Each panel shows different classifications of four types of spectral shapes: (a) Lower band only, (b) Upper band only, (c) Banded, and (d) No-gap. In all panels, the vertical black dashed line indicates $0.5 f_{ce}$ and the horizontal red dashed-and-dotted line represents the threshold power spectral density, $p_{th} = 10^{-6} \text{ nT}^2/\text{Hz}$. In panels (c) and (d), $10^{-1.5} p_L$ and $10^{-1.5} p_U$ are shown by the horizontal blue dashed lines.

3 Results

Plasma properties in the near-Moon space vary significantly in time and space. Consequently the wave excitation condition also changes, and it is necessary to separate the statistics by the plasma environment. First, we organize the data into coordinates relevant to the field line connection to the Moon under a straight field line assumption (Figure 2), because the connection of the observation point to the Moon by magnetic field lines is suggested to be a key controlling factor for the excitation of whistler-mode waves (Halekas, Poppe, Farrell, et al., 2012; Harada et al., 2014, 2015). As illustrated in Figure 2b, for a given spacecraft position and a measured magnetic field vector, we extrapolate a straight field line from the spacecraft. We calculate the minimum distance between the straight field line and the center of the Moon (hereafter termed “B distance”), and the distance from the spacecraft to the point at which the field line is closest to the center of the Moon (“SC distance”). If we display this coordinate system with the SC and B distances on the X and Y axes, respectively, a simple condition of $Y < 1R_L$ indicates the magnetic field line connection to the Moon under the straight field line assumption. In practice, the assumption may not be valid due to the field line curvature, and the boundary of connected and unconnected conditions may not be perfectly distinct at $Y = 1R_L$. Figure 2a shows the SC distance–B distance distribution of the occurrence rate (defined as the fraction of observed spectra showing the wave events in each bin) of all events for all observations, regardless of the event types. The occurrence rate increases over an order of magnitude for $Y < 1R_L$, indicating that the field-line connection controls the excitation of the whistler-mode waves. As the SC distance increases, the boundary of high- and low-occurrence rate regions becomes increasingly blurred, as expected from field lines with finite curvature. Nevertheless, the enhanced occurrence rate at $Y < 1R_L$ is clearly visible even at $X > 10R_L$ around the apoapsis of ARTEMIS, and hereafter we classify events with $Y < 1R_L$ as Moon-related wave events.

Next, the external plasma environment is separated, to first order, according to the position of the Moon. For simplicity and full use of available FFT data, we use the GSE longitude, θ_{GSE} , of the Moon (full moon as seen from the Earth corresponding to $\theta_{GSE} = 0^\circ$) and classify the plasma regime into three categories, the solar wind (SW; $53^\circ < \theta_{GSE} < 293^\circ$), magnetosheath (MS; $27^\circ < \theta_{GSE} < 53^\circ$ and $293^\circ < \theta_{GSE} < 327^\circ$), and magnetotail (MT; $\theta_{GSE} < 27^\circ$ and $327^\circ < \theta_{GSE}$), based on the average ion properties derived from long-term ARTEMIS data by Poppe et al. (2018). It should be noted that

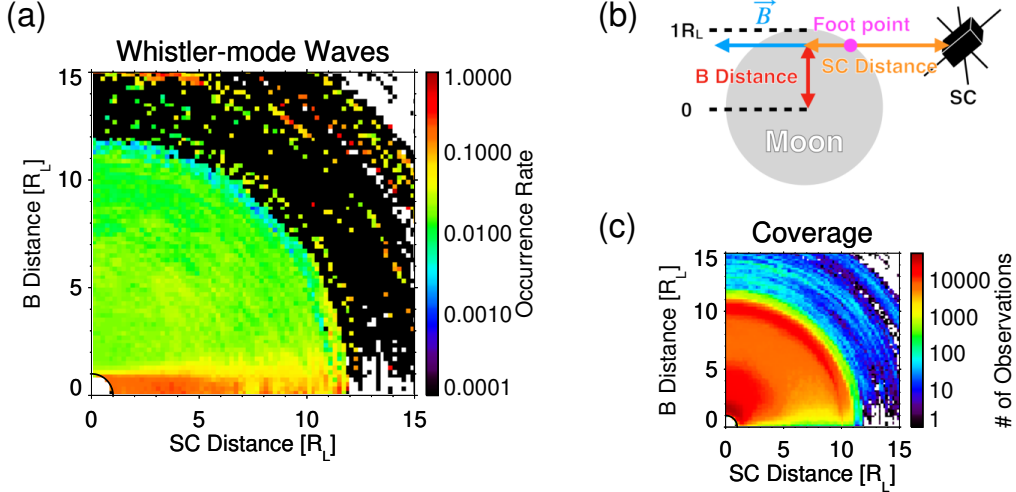


Figure 2. (a) Occurrence rate distribution of all types of events in all regions. The Y-axis represents the minimum distance in lunar radii between the magnetic field line and the center of the Moon, and the X-axis represents the distance in lunar radii from the spacecraft to the point at which the field line is closest to the center of the Moon. (b) Schematic illustration of the coordinate system used in panel (a). (c) Number of all observations shown in the same format as panel (a).

208 this classification is only an approximation and each category is likely to include some
 209 observations in adjacent plasma regimes.

210 Figures 3-5 show the occurrence rate distributions in the same format as Figure
 211 2a, except that they are classified by the external plasma environment and wave spec-
 212 tral shapes. Although the upper band only events in the solar wind (Figure 3b) and mag-
 213 netosheath (Figure 4b) as well as the banded events in all regions (Figures 3c, 4c, and
 214 5c) are too rare to discern any meaningful trend, the occurrence rates of the other clas-
 215 sifications clearly increase for $Y < 1R_L$. The higher occurrence rates within $Y < 1R_L$
 216 confirm once again that magnetic field line connection to the Moon is an important fac-
 217 tor in the excitation of whistler-mode waves, and in the following analysis we will focus
 218 on these Moon-related wave events at $Y < 1R_L$. We note that a relative increase is ob-
 219 served in the occurrence rate of lower band only events at $Y > 1R_L$ in the magnetosheath
 220 (Figure 4a), possibly due to the detection of lion roars originally present in the background
 221 magnetosheath plasma (Smith & Tsurutani, 1976). As shown in Figure 6, the number

Solar Wind

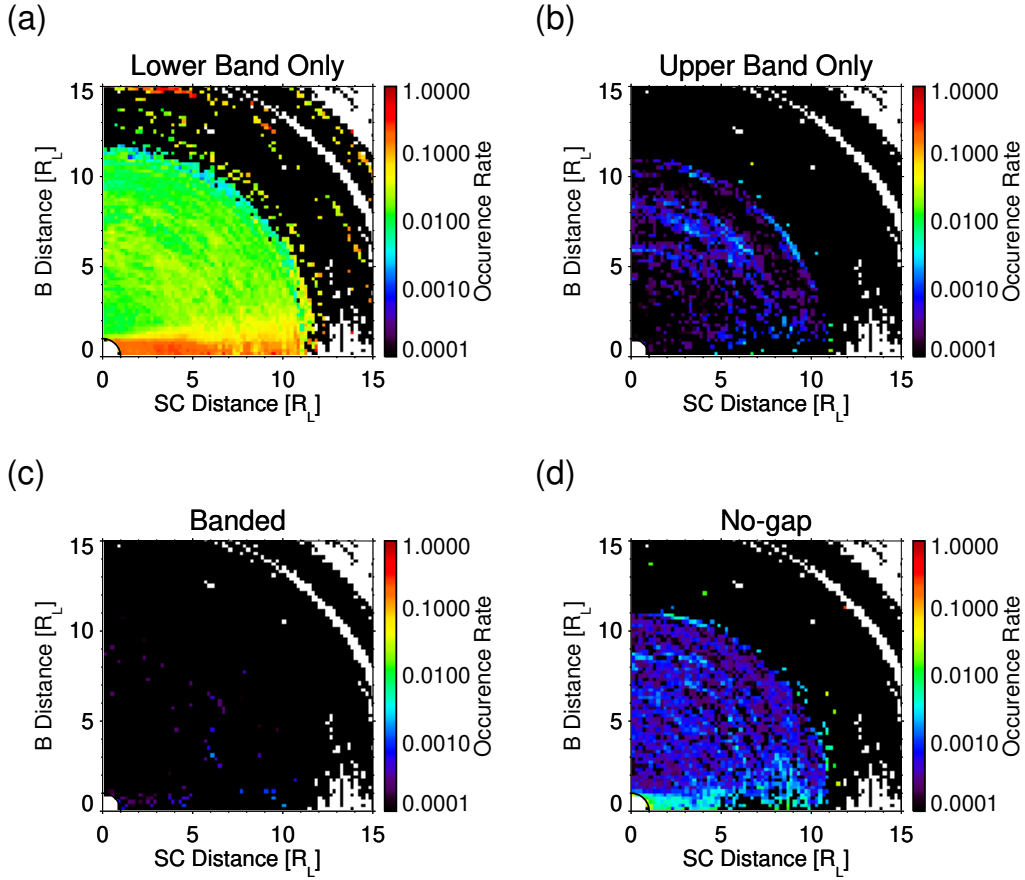


Figure 3. Occurrence rate distributions of four types of whistler-mode wave events in the solar wind. Each panel is in the same format as Figure 2

222 of observation points, which represent the denominator of the occurrence rate, is suffi-
 223 ciently large within $X < \sim 11R_L$.

224 Solar radiation is also an important driver in the lunar plasma environment. For
 225 example, photoelectrons are emitted from the dayside lunar surface, leading to positive
 226 surface charging on the day side of the Moon. On the night side, in addition to nega-
 227 tive charging of the lunar surface driven by a predominant ambient electron current, the
 228 lunar wake is formed downstream of the solar wind. Hence, we divide the Moon-related
 229 events into dayside and nightside events based on the solar zenith angle at the foot point
 230 of the magnetic field line. Events with solar zenith angles $< 90^\circ$ ($> 90^\circ$) are classified

Magnetosheath

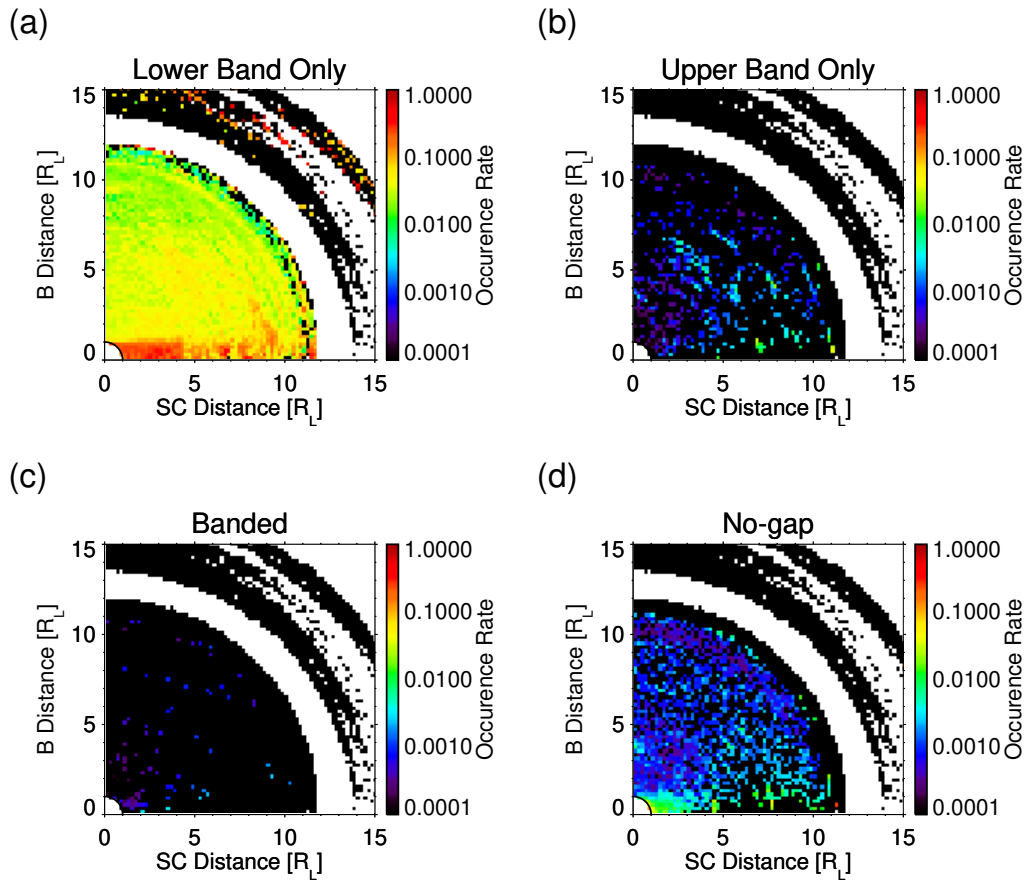


Figure 4. Occurrence rate distributions of four types of whistler-mode wave events in the magnetosheath. Each panel is in the same format as Figure 2

Magnetotail

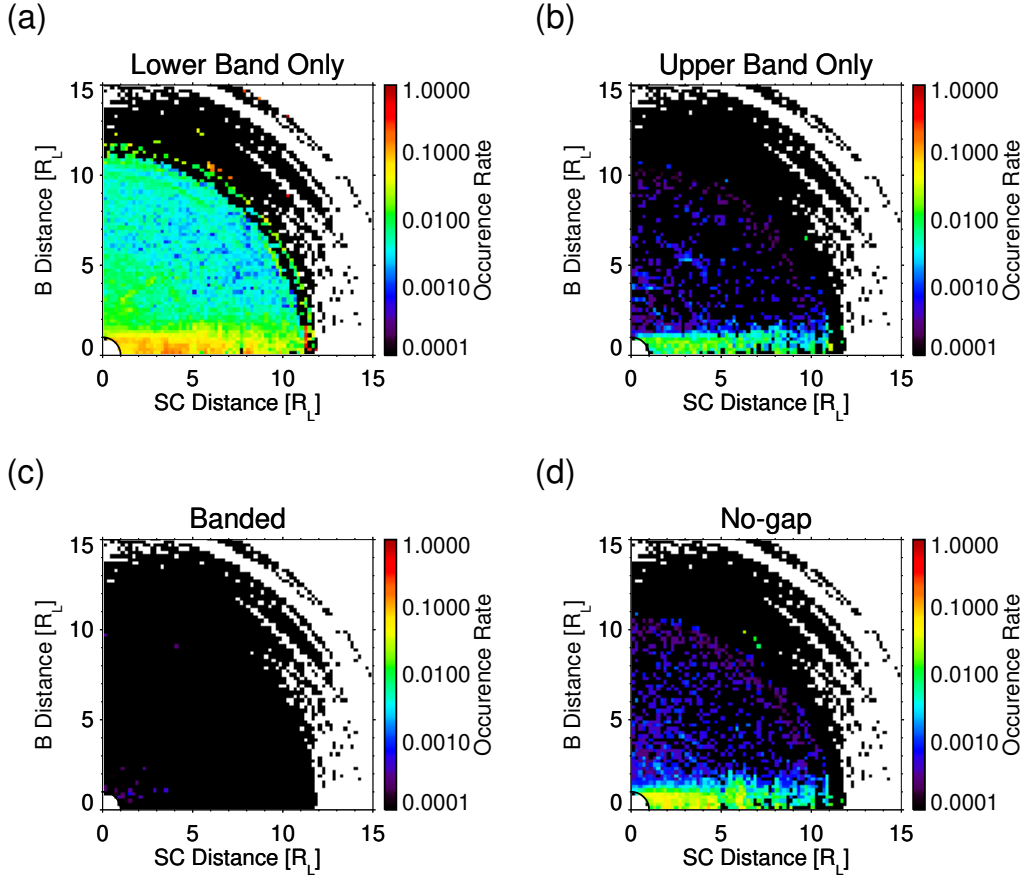


Figure 5. Occurrence rate distributions of four types of whistler-mode wave events in the magnetotail. Each panel is in the same format as Figure 2

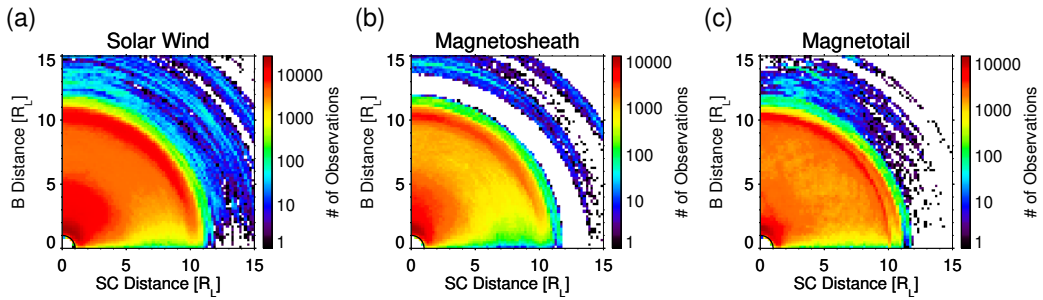


Figure 6. Observation point distributions in the solar wind, magnetosheath, and magnetotail. Each panel is in the same format as Figure 2 except that the color indicates the total number of observations in each bin.

Table 1. Number (occurrence rate) of whistler-mode wave events classified by day/night at foot point of the magnetic field line and the location of the Moon.

Day/Night	Region	Data points	Wave events
Day	SW	360,289	81,005 (22.5%)
	MS	86,961	28,068 (32.3%)
	MT	165,105	21,839 (13.2%)
Night	SW	248,591	14,658 (5.90%)
	MS	77,833	6,362 (8.12%)
	MT	110,186	8,462 (7.68%)

231 as dayside (nightside) events. Tables 1 and 2 show the results for the day-night condi-
 232 tions subdivided by the external plasma environment.

233 First, we point out that very few banded events are identified while the no-gap events
 234 rank the second most common type for any circumstances shown in the rows of Table
 235 2. The banded to no-gap ratio of <0.05 is markedly different from $\sim 2-3$ in the terres-
 236 trial inner magnetosphere (Teng et al., 2019; Gao et al., 2019). We note that this dif-
 237 ference is unlikely to arise from the differences in the algorithm or data as demonstrated
 238 in Supporting Information. Second, the ratio of upper band only to no-gap events is larger
 239 in the magnetotail than in the other two regions regardless of day or night (Table 2), in-
 240 dicated that upper band only events are rarely observed in the solar wind and in the
 241 magnetosheath. Third, in comparison between the day and night conditions, the occur-
 242 rence rates are clearly higher on the day side (Table 1).

243 To investigate the influence of the lunar magnetic anomalies on Moon-related waves,
 244 we map the occurrence rates in the selenographic coordinates based on the foot point
 245 longitude and latitude, separately for the dayside and nightside events. Figures 7-9 show
 246 the occurrence rates in the selenographic coordinates in the solar wind, magnetosheath,
 247 and magnetotail. The contours in solid black and magenta lines indicates a crustal field
 248 strength of 2 nT at a 30 km altitude evaluated by the lunar magnetic anomaly model
 249 of Tsunakawa et al. (2015). Note that the observation points in these distributions are
 250 heavily biased in longitude owing to the geometrical constraints of the lunar orbit (pan-
 251 els a and f in Figures 7-9). Also note that, as only few events are identified, no mean-

Table 2. Number (ratio) of four types of events classified by day/night at foot point of the magnetic field line and the location of the Moon.

Day/Night	Region	Lower	Upper	Banded	No-gap
Day	SW	78,656 (97.1%)	44 (0.05%)	43 (0.05%)	2,262 (2.79%)
	MS	26,975 (96.1%)	33 (0.12%)	19 (0.07%)	1,041 (3.71%)
	MT	11,659 (53.4%)	2,842 (13.0%)	13 (0.06%)	7,325 (33.5%)
Night	SW	14,453 (98.6%)	18 (0.12%)	7 (0.05%)	180 (1.23%)
	MS	6,180 (97.1%)	38 (0.60%)	6 (0.09%)	138 (2.17%)
	MT	7,546 (89.2%)	295 (3.49%)	2 (0.02%)	619 (7.32%)

252 ingful trend can be discerned for the upper band only and banded (Figures 7c, 7d, 7h
253 and 7i) and no-gap (Figure 7j) in the solar wind, the upper band only and banded (Fig-
254 ures 8c, 8d, 8h and 8i) in the magnetosheath, and the banded (Figures 9d and 9i) in the
255 magnetotail. In the other cases, the occurrence rates generally decrease near the mag-
256 netic anomalies as suggested by Harada et al. (2014). However, we also find two features
257 that contradict this trend: (i) there exists a high occurrence area around Reiner Gamma
258 (-20° to 20° latitudes and -90° to -60° longitudes) regardless of the lunar circumstances
259 and the spectral shapes; and (ii) for the lower band only events on the night side in the
260 solar wind and magnetosheath (Figures 7g and 8g), high occurrence rates are seen in sev-
261 eral longitude and latitude bands with no apparent association with magnetic anoma-
262 lies.

263 4 Discussion

264 4.1 Two-band structure formation

265 The statistical results show that no-gap whistler-mode waves are much more com-
266 mon than banded waves with detectable gaps around the Moon, suggesting that the $0.5f_{ce}$
267 gap generation mechanisms are not as effective around the Moon as they are in the ter-
268 restrial inner magnetosphere. Here we discuss the applicability of the gap generation sce-
269 narios to the Moon-related whistler-mode waves.

Solar Wind

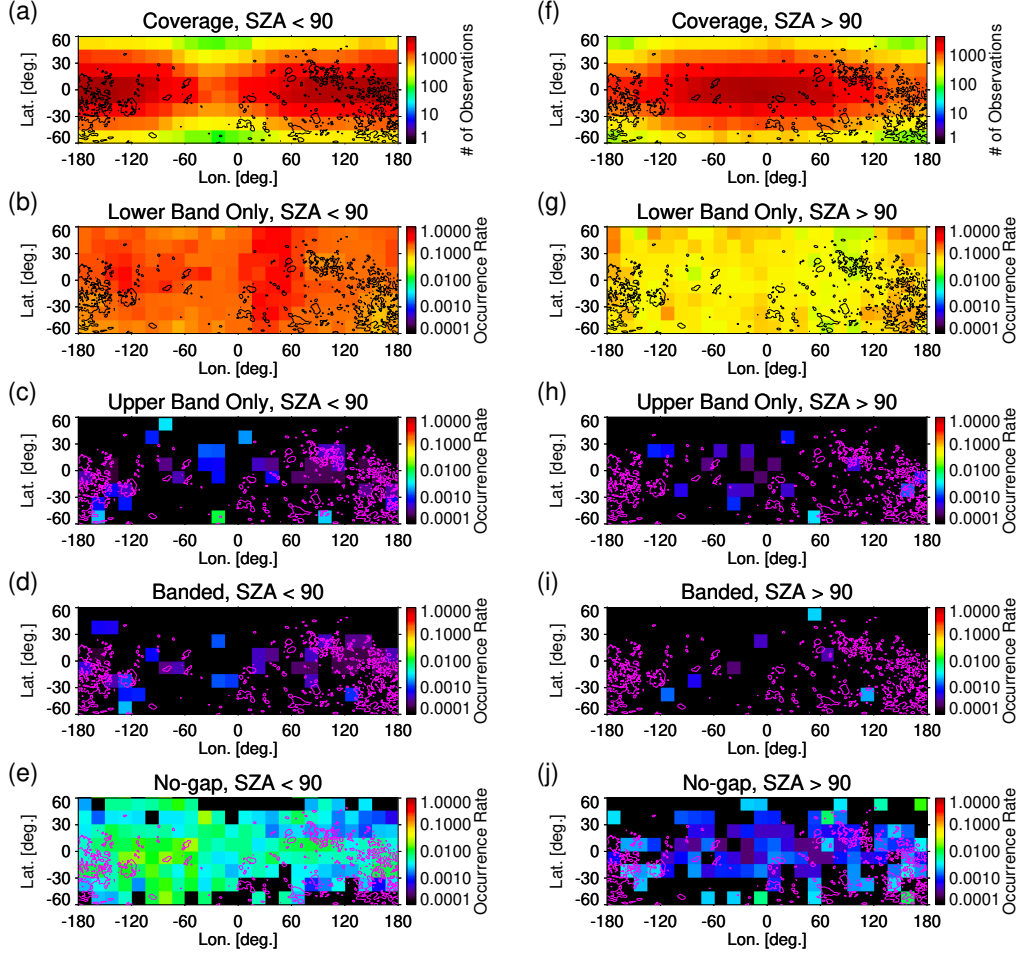


Figure 7. (a) Number of observations when the background magnetic field line is connected to the day side of the Moon in the solar wind and (b-e) occurrence rates of four types of whistler-mode wave events as a function of selenographic locations of the field line foot point. Panel (f) and Panels (g-j) are the same data as panel (a) and panels (b-e) except that the background magnetic field line is connected to the night side of the Moon. The contours in solid black and magenta lines indicates a crustal field strength of 2 nT at a 30 km altitude evaluated by the lunar magnetic anomaly model of Tsunakawa et al. (2015).

Magnetosheath

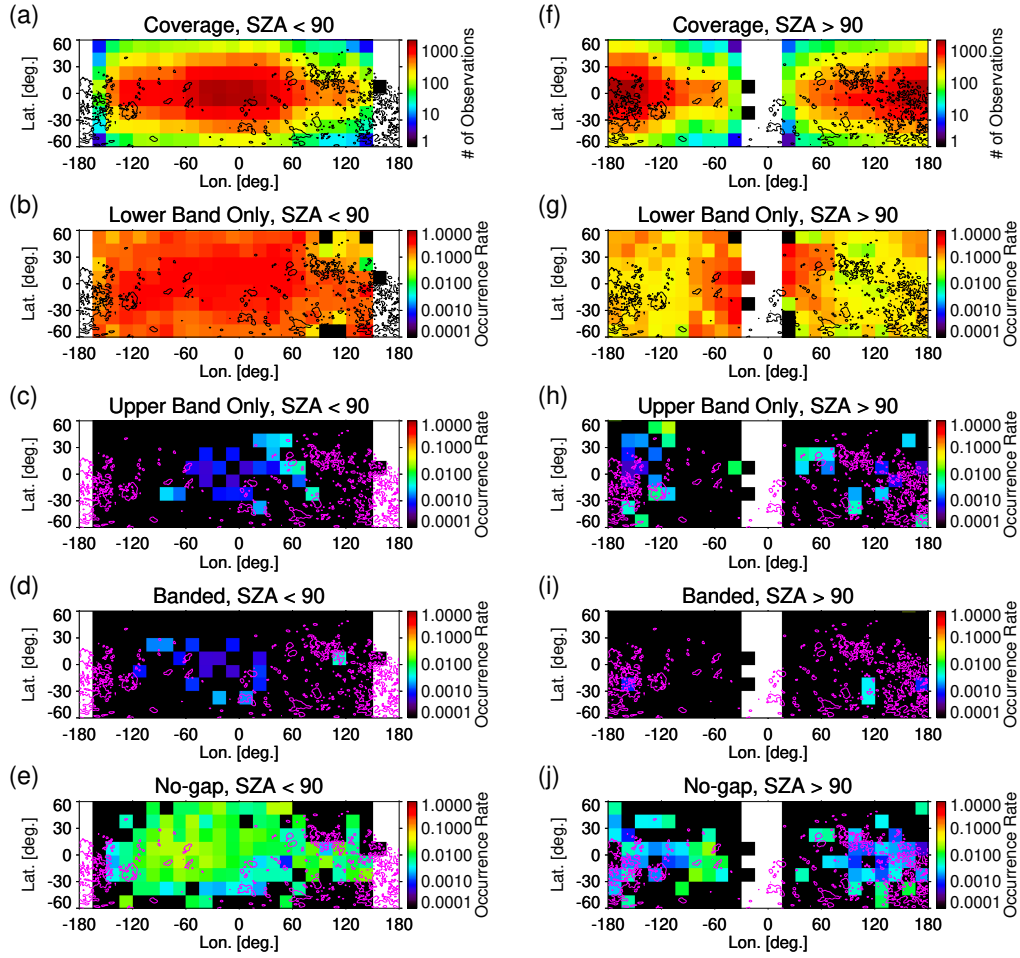


Figure 8. Selenographic distributions of observation points and event occurrence rates in the magnetosheath in the same format as Figure 7.

Magnetotail

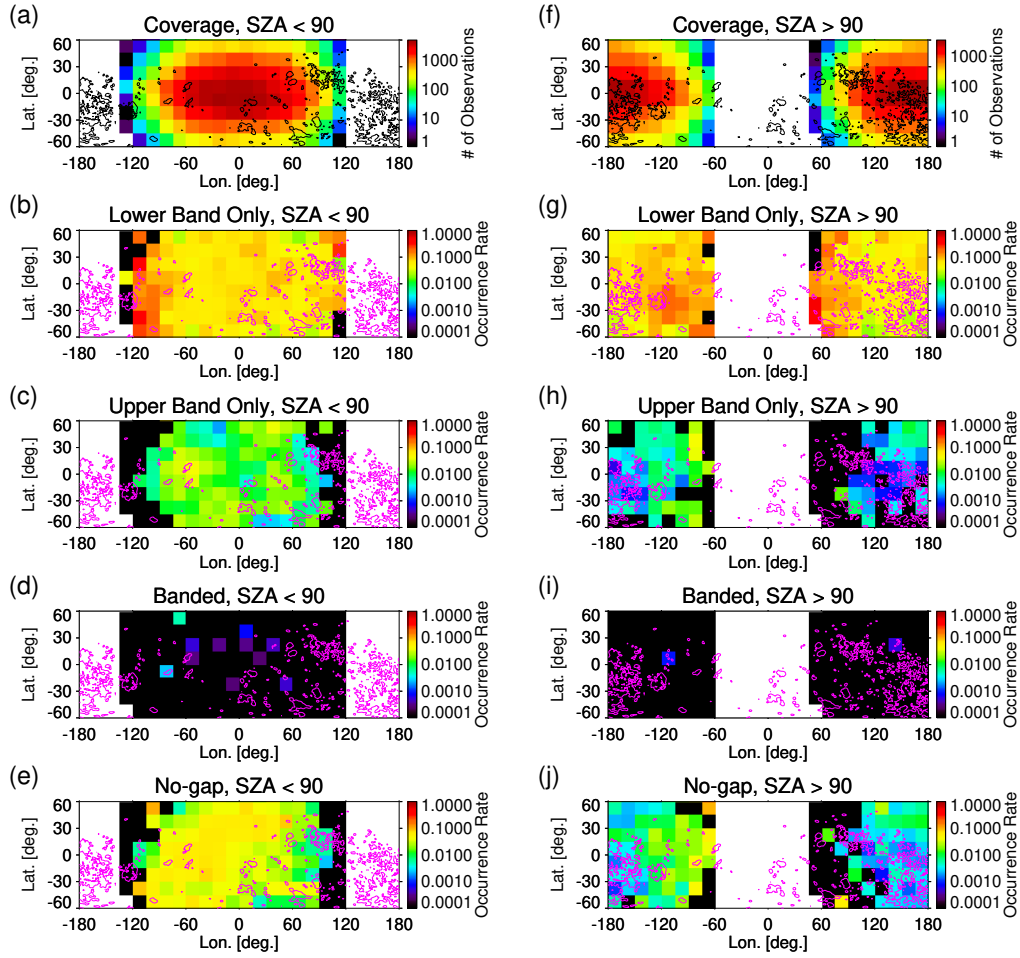


Figure 9. Selenographic distributions of observation points and event occurrence rates in the magnetotail in the same format as Figure 7.

270 First, in the Landau damping gap formation scenario for terrestrial chorus emis-
 271 sions (Tsurutani & Smith, 1974; Omura et al., 2009), a broad band wave is excited in
 272 the equatorial source region and subsequently propagates to higher latitudes, widening
 273 the gap at the local $0.5f_{ce}$ due to the increase of the field strength. In contrast, at least
 274 for typical conditions in the solar wind and magnetotail, one of the possible explanations
 275 for the absence of banded events could be provided by the $0.5f_{ce}$ variation being too small
 276 to generate a detectable gap. To a first-order approximation, the field-aligned gradient
 277 of the magnetic field strength around the Moon is expected to be negligible. For typ-
 278 ical conditions in the solar wind, incompressible Alfvénic disturbances prevail, and the
 279 field strength fluctuations are small (Khabibrakhmanov & Summers, 1997). In the mag-
 280 netotail at the lunar orbit 60 Earth radii downstream of the Earth, the magnetic field
 281 lines are highly stretched along the Sun-Earth line, and the magnetic field strength may
 282 be more or less uniform along the field lines except for dynamically formed structures
 283 (e.g., plasmoids) during geomagnetically disturbed conditions. On the other hand, since
 284 compressible disturbances dominate in the magnetosheath, as typified by the mirror mode
 285 structure, the gradient of the magnetic field strength should be large (Tsurutani et al.,
 286 1982), and this argument cannot explain why the banded waves were not observed in the
 287 magnetosheath. In order to assess the effectiveness of the gap formation by Landau damp-
 288 ing, the magnetic field gradient around the Moon should be quantitatively evaluated from
 289 observations in each plasma regime, but this is beyond the scope of this paper.

290 Another explanation for the absence of a Landau damped gap is that the waves
 291 are generally observed inside the source region because the whistler-mode waves travel
 292 toward the lunar surface in cyclotron resonance with upward traveling electrons. This
 293 situation is essentially different from the terrestrial chorus emissions, for which the waves
 294 are commonly observed after the propagation away from the source region localized near
 295 the magnetic equator. Therefore, the formation of a deep gap by Landau damping dur-
 296 ing propagation is unlikely to occur for the Moon-related whistler-mode waves, because
 297 even if Landau damping did occur, the damped area in the spectrum would be imme-
 298 diately filled by further wave excitation.

299 A simple extrapolation of the lower band cascade scenario for terrestrial chorus emis-
 300 sions to the Moon-related whistler-mode waves cannot explain the absence of banded events.
 301 In the lower band cascade scenario in the Earth’s magnetosphere, the lower band wave
 302 amplitude exceeding ~ 100 pT is a necessary condition for the formation of a two-band

303 structure by subsequent excitation of the upper band waves (Gao et al., 2016). Figure
 304 3 in Sawaguchi et al. (2021) shows a lower band only event with rising tone elements ob-
 305 served around the Moon, whose magnetic field amplitude exceeds 100 pT, seemingly sat-
 306 isfying the upper band excitation threshold. In our statistical results, banded waves are
 307 almost absent, despite the intensity of observed waves as large as those in the Earth mag-
 308 netosphere. Note, however, that in the lower band cascade scenario, the upper band may
 309 be electrostatic and the two-band structure may be seen only in the electric field (Gao
 310 et al., 2019). Since our analysis did not examine the electric field, we cannot distinguish
 311 lower band only waves from this type of banded waves caused by the cascade scenario.

312 We next discuss the scenario proposed in Fu et al. (2014), in which the two elec-
 313 tron components excite the lower and upper bands separately. There seems to be gen-
 314 erally no mechanism to separate electrons with temperature anisotropy into two com-
 315 ponents at the Moon, and we conclude that this two component scenario is not appli-
 316 cable to the Moon-related whistler-mode waves. Considering that the electron anisotropy
 317 at the Moon originates from a loss cone due to electron absorption at the lunar surface,
 318 it is implausible that the driving anisotropic electrons consist of two separated compo-
 319 nents at high and low energies, and such peculiar electron distributions have not been
 320 reported so far to the best of our knowledge.

321 4.2 An example of banded events

322 For more detailed discussion on the gap formation mechanisms, we next look at a
 323 specific example shown in Figure 10 among the rare banded events. This event was ob-
 324 served in the solar wind (Figures 10a, 10e, and 10i), P1 and P2 happened to be located
 325 on nearby magnetic field lines (Figure 10a), and P1 and P2 observed the loss cone of the
 326 upward (parallel) electrons formed by lunar surface absorption (Figures 10f and 10j) and
 327 the electromagnetic waves below and above $0.5 f_{ce}$ (Figures 10g and 10k). One of the
 328 most remarkable features is the temporary disappearance of the lower band wave and
 329 the loss cone structure of the upward-traveling electrons observed by P1 at around 21:13
 330 UT (indicated by the arrows in Figures 10j and 10k), indicating that the magnetic field
 331 line was disconnected from the Moon at this timing. Simultaneously, the change in the
 332 direction of the background magnetic field was observed (Figure 10h). The magenta ar-
 333 rows in Figure 10b indicate the three data points that were classified as banded events.
 334 While the lower band was nearly continuously observed, the upper band signatures were

335 only intermittently detected. The wave intensity of the lower band decreased from 21:44:40
 336 to 21:45:00 UT, and at the same time the size of the loss cone of 100 to 500 eV electrons
 337 became narrower (Figures 10b and 10d). Based on calculation of the resonance veloc-
 338 ity, these electrons shown in Figure 10d corresponds well to the resonant electrons for
 339 the lower band. In Figure 10b, upper band waves were also observed just before the banded
 340 events indicated by the arrows, although their intensity was lower than the event selec-
 341 tion threshold. These upper band waves have no apparent association with the pitch an-
 342 gle distributions of 10-20 eV electrons (Figure 10c), which are expected to be in cyclotron
 343 resonance with the waves at $\sim 0.5\text{--}0.6f_{ce}$. Looking again at the dynamic spectra in Fig-
 344 ures 10g and 10k, we can see intermittent observations of the upper band while the lower
 345 band continues for a few to tens of minutes. The frequency of the “upper band” wave
 346 component with small intensity varied greatly in the time series, and in fact, its frequency
 347 dropped below $0.5f_{ce}$ for some instances. It is also noteworthy that the upper band-like
 348 component was observed even around 21:13 UT, when the magnetic field line was tem-
 349 porarily disconnected as mentioned above.

350 We now discuss possible generation mechanisms of the two-band structure in this
 351 event. The Landau damping scenario, in which an originally continuous rising tone com-
 352 ponent extending over both bands is split into two by Landau damping, is inadequate
 353 to explain the uncorrelated generation of the lower band and upper band as seen in this
 354 event. In the lower band cascade scenario, the upper band should be excited as a har-
 355 monic about twice as high as the lower band, but this is not the case for this event be-
 356 cause the frequencies of the lower band and upper band are obviously not harmonically
 357 related. The scenario with separate wave excitation by the two anisotropic electron com-
 358 ponents is hard to be reconciled with the observed electron distributions. Considering
 359 these facts, we speculate that this event may be a coincident detection of lower band whistler-
 360 mode waves excited at the field line foot point and higher frequency whistler-mode waves
 361 propagating from a different wave source, and the two waves are coincidentally present
 362 at the observed location. In the P1 data, the connection of the magnetic field lines to
 363 the Moon is lost around 21:49 UT, and concurrently the intense component of the lower
 364 band is no longer observed, while the weak wave component at a relatively high frequency
 365 at ~ 150 Hz ($0.4f_{ce}$) is continuously observed until about four minutes later (Figures 10j
 366 and 10k). Moreover, no upper band waves were observed in P2 before 21:38 UT (Fig-
 367 ure 10g), when the field line connection started as is evident from the appearance of the

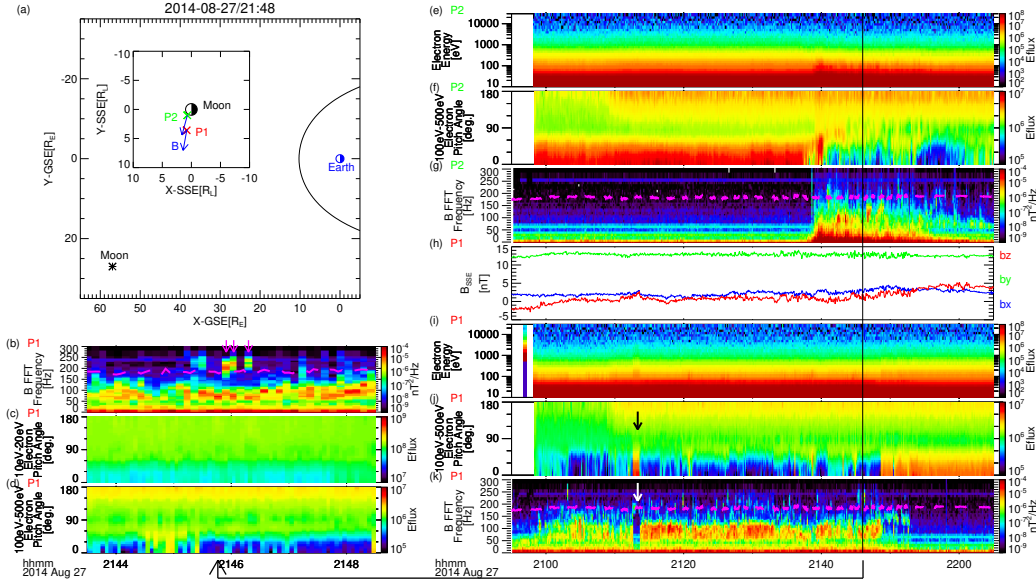


Figure 10. ARTEMIS observations of banded wave events on August 27, 2014. (a) The position of the Moon in the geocentric solar ecliptic (GSE) coordinate system, where the blue circle, the black asterisk, and the black line represent the Earth, the Moon, and a typical magnetopause location (Shue et al., 1997), respectively. The inset shows the positions of the probes in the selenocentric solar ecliptic (SSE) coordinate system, where the black circle, and red and green X-marks, and blue arrows represent the Moon, P1 and P2, and magnetic field direction, respectively. Time series data from ARTEMIS P1 at 21:43:30–21:48:30 UT of (b) magnetic wave spectra and pitch angle spectra of (c) 10–20 eV and (d) 100–500 eV electrons in units of differential energy flux (labeled “Eflux” for short, eV/cm²/sr/s/eV). Time series data from ARTEMIS P1 and P2 at 20:55–22:05 UT of (e, i) energy spectra of electrons in units of differential energy flux, (f, j) pitch angle spectra of 100–500 eV electrons in units of differential energy flux, (g, k) magnetic wave spectra, (g) magnetic fields in the SSE coordinate system. The data shown in panels (h–k) and panels (e–g) are obtained by P1 and P2, respectively. The dashed magenta lines in panels (g) and (k) represent half the electron cyclotron frequency. Banded events are denoted by the magenta arrows in panel (b).

368 electron loss cone (Figure 10f), indicating no clear wave activity in the pristine solar wind.
 369 These results suggest that whistler-mode waves generated on another magnetic field line
 370 connected to the lunar surface at a different foot point may have propagated across the
 371 magnetic field line with an oblique propagation angle. Unfortunately, no burst-mode wave-
 372 form magnetic field data are available for this time, so the propagation angle cannot be
 373 examined.

374 **4.3 Dependences on the external and local plasma environments**

375 In Section 3, notable differences are identified in the occurrence rates of whistler-
 376 mode wave events depending on the magnetic connection to the Moon, the position of
 377 the Moon, and the day/night condition and the selenographic location of the field-line
 378 foot point. First, it is directly demonstrated from the occurrence rates that the magnetic
 379 field line connection to the Moon is a dominant controlling factor in whistler-mode wave
 380 excitation, also consistent with case studies and average wave power statistics in the pre-
 381 vious studies (Halekas, Poppe, Farrell, et al., 2012; Harada et al., 2014).

382 Next, on field lines connected to the night side of the Moon, the wave occurrence
 383 rate is smaller than the day side regardless of the frequency band and the position of the
 384 Moon. Also, the occurrence rate of upper band waves is suppressed in the solar wind and
 385 magnetosheath compared to that in the magnetotail. We explain these suppressions by
 386 small anisotropy resulting from enhanced reflection of electrons above the lunar surface.
 387 The nightside lunar surface is negatively charged, and the negative electrostatic poten-
 388 tial reflects incident electrons with low parallel energies. As the reflected electrons fill
 389 the otherwise empty loss cone, the electrostatic reflection reduces the effective temper-
 390 ature anisotropy, possibly leading to the suppressed wave occurrence on field lines con-
 391 nected to the nightside lunar surface. The small anisotropy at low energies resulting from
 392 the electrostatic reflection would lead to suppression of high frequency whistler-mode waves.
 393 This can explain the reduced relative occurrence of upper band events on the night side
 394 in the magnetotail with respect to that on the day side in the magnetotail. The low oc-
 395 currence of upper band events on the day side in the solar wind and magnetosheath com-
 396 pared to that in the magnetotail could be explained in a similar manner; for magnetic
 397 reflection (or electrostatic reflection if a downward electric field exists) from the day side
 398 of the Moon in a fast moving plasma such as the solar wind and magnetosheath flow,
 399 the reflected electrons are effectively accelerated in the plasma reference frame because

400 of the moving obstacle effect (Halekas, Poppe, Farrell, et al., 2012; Halekas, Poppe, De-
 401 lory, et al., 2012). This effect shifts the reflected component toward higher parallel ve-
 402 locities in the plasma frame, effectively reducing the electron anisotropy at lower ener-
 403 gies and suppressing whistler-mode wave excitation at higher frequencies such as upper
 404 band events.

405 We observe generally reduced occurrence rates of Moon-related wave events on field
 406 lines connected to magnetic anomalies. This is consistent with the reduced electron anisotropy
 407 by the magnetic mirror reflection as proposed by Harada et al. (2014). However, we pointed
 408 out the two notable exceptions. The first exception is the enhanced occurrence rate near
 409 latitudes from -20° to 20° and longitudes from -90° to -60° , where several isolated mag-
 410 netic anomalies exist, including a strong magnetic anomaly called Reiner Gamma around
 411 latitude 8° and longitude -58° (Kurata et al., 2005; Tsunakawa et al., 2015). This may
 412 imply that the spatial extent of the magnetic anomalies could play a role in the wave ex-
 413 citation, but it remains unclear why the magnetic connection to these isolated magnetic
 414 anomalies is favorable for the wave occurrence as opposed to spatially extended magnetic
 415 anomalies.

416 The second exception is the lower band only event on the night side of the solar
 417 wind and magnetosheath (Figures 7g and 8g). The occurrence rate distributions in these
 418 cases show no clear correlation with the magnetic anomalies, but rather show enhanced
 419 occurrence at certain latitude and longitude bands. This could result from sampling bias
 420 related to solar zenith angles as described in the following. For example, high latitude
 421 regions are biased toward solar zenith angles near 90° . Similarly, because of tidal lock-
 422 ing and the limited range of lunar phase in the solar wind, there are fewer observations
 423 at 0° longitude on the near side with solar zenith angles near 0° in the solar wind. This
 424 deviation of the solar zenith angle could affect the wave occurrence rate because of the
 425 gradual variation in the magnitude of the aforementioned electron anisotropy due to the
 426 transition of the lunar surface potential near the terminator (Halekas et al., 2008).

427 The relationship between the foot point solar zenith angle and the occurrence rates
 428 of Moon-related wave events is shown in Figure 11. For observations in the solar wind,
 429 magnetosheath, and magnetotail, the occurrence rates were calculated by dividing the
 430 number of identified events in each bin by the number of all observations in the bin, shown
 431 by the solid (dashed) magenta lines for unmagnetized (magnetized) regions. Here we cat-

432 egorize the unmagnetized (< 2 nT) and magnetized (≥ 2 nT) regions according to
 433 the crustal field strength at the foot point longitude and latitude evaluated at a 30 km
 434 altitude by the lunar magnetic anomaly model of Tsunakawa et al. (2015). We only show
 435 the lower band only events, which have a relatively large number of events. The over-
 436 all trend is that the occurrence rate is higher on the day side (at smaller solar zenith an-
 437 gles) and lower on the night side as already discussed. Additionally, the occurrence rates
 438 of both unmagnetized and magnetized regions decrease with increasing solar zenith an-
 439 gles on the night side in the solar wind and magnetosheath. The gradual decrease of the
 440 occurrence rates from 90° to 120° could explain the high-latitude enhancement of the
 441 occurrence rates seen in Figures 7g and 8g and the nearside enhancement in Figure 8g.
 442 In addition, the difference in occurrence rates between the unmagnetized and magne-
 443 tized regions is smaller on the night side than on the day side. This could be because
 444 the electrostatic reflection from the negatively charged nightside surface occurs for both
 445 unmagnetized and magnetized regions, leading to relatively small differences in the ef-
 446 fective electron anisotropy between the unmagnetized and magnetized regions.

447 Another notable signature is an enhancement of the occurrence rates near the ter-
 448 minator at 90° solar zenith angle in the magnetotail (Figure 11c). This could result from
 449 another sampling bias in the background plasma conditions. In the B_x (sunward/tailward
 450 component) dominant magnetotail lobes, the equatorial probe has a small chance of mag-
 451 netic connection to the terminator during its orbit. Meanwhile, for more variable mag-
 452 netic field directions in the plasma sheet, particularly during geomagnetically disturbed
 453 conditions, the probe has a higher probability of magnetic connection to the near-terminator
 454 surface. Consequently, the near-terminator foot point observations are disproportion-
 455 ately obtained in the plasma sheet, where intense, Moon-related whistler-mode waves
 456 are observed (Halekas, Poppe, Farrell, et al., 2012; Harada et al., 2014), possibly explain-
 457 ing the apparent increase of the near-terminator occurrence rates in the magnetotail.

458 5 Conclusions

459 In this study, we identified Moon-related whistler-mode waves from 9 years of ARTEMIS
 460 data and classified their spectral shapes in a fully automated manner, thereby statisti-
 461 cally investigating the occurrence rates of four types of events: lower band only, upper
 462 band only, banded, and no-gap. The results are summarized as follows. (i) The occur-
 463 rence rate of whistler-mode waves is enhanced over an order of magnitude on magnetic

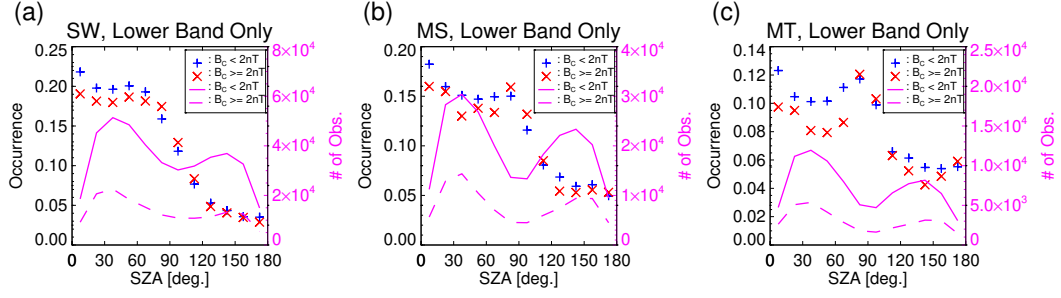


Figure 11. Occurrence rates of Moon-related lower band only wave events as functions of solar zenith angles observed in (a) the solar wind, (b) magnetosheath and (c) magnetotail; blue and red marks are for unmagnetized and magnetized regions. Solid (dashed) magenta lines show the number of all observations in each bin for unmagnetized (magnetized) regions.

464 field lines connected to the Moon (Moon-related wave events), indicating that the mag-
 465 netic connection is a key factor for wave excitation. (ii) Banded events were rarely ob-
 466 served in the Moon-related wave events (occurrence ratios of banded/no-gap events < 0.05
 467 at the Moon as opposed to $\sim 2-3$ in the terrestrial inner magnetosphere). (iii) The wave
 468 occurrence rate decreases when the magnetic field line is connected to the lunar night
 469 side compared to the day side, suggesting that the excitation of the whistler-mode waves
 470 is suppressed by lower anisotropy of upward traveling electrons resulting from the neg-
 471 ative potential of the nightside lunar surface. (iv) The occurrence rate of the upper band
 472 waves is relatively low in the solar wind and magnetosheath in comparison to that in the
 473 magnetotail, suggesting that the excitation of high-frequency waves is suppressed by a
 474 lower temperature anisotropy of low-energy electrons in the plasma frame resulting from
 475 the moving obstacle effect. (v) The wave occurrence rates are generally decreased when
 476 the field line is connected to the lunar magnetic anomalies, which can be explained by
 477 lower anisotropy of electrons magnetically reflected from strong crustal magnetic fields
 478 as suggested by Harada et al. (2014), but we also identified exceptions of high occurrence
 479 rates near isolated, strong magnetic anomalies (e.g. Reiner Gamma).

480 The absence of banded events in the vicinity of the Moon makes a stark contrast
 481 to the common presence of a $0.5f_{ce}$ gap for the chorus emissions in the terrestrial inner
 482 magnetosphere. These results suggest that the formation mechanisms for the two-band
 483 structure are much less effective in the lunar environment than those operating in the

484 terrestrial inner magnetosphere. Specifically, we infer that the two-band structure for-
485 mation by Landau damping or two electron components is not applicable to the near-
486 Moon space given the plasma properties and magnetic field structure therein. Meanwhile,
487 many of the detected wave amplitudes apparently exceed the wave-intensity threshold
488 of the lower band cascade mechanism described in Gao et al. (2016), implying that some
489 unidentified factors must be elucidated in order to account for the absence of banded events.
490 It is notable that another characteristic signature of the chorus emissions, rising tone el-
491 ements resulting from nonlinear growth, is present even around the Moon (Sawaguchi
492 et al., 2021).

493 Additionally, we propose that the variability of wave spectral shapes arises from
494 the varying shape of the electron velocity distribution function, which provides a free en-
495 ergy source for the excitation of whistler-mode waves. This variability can be caused by
496 different degrees of deformation of electron velocity distributions by electrostatic and mag-
497 netic mirror reflections depending on the lunar surface charging, crustal magnetic field
498 strength, and moving obstacle effect. Taken together, the presented results highlight the
499 complexity and diversity of lunar plasma and electromagnetic environments, and reveal
500 the similarities and differences between the lunar and terrestrial whistler-mode waves,
501 thereby reinforcing the idea that the Moon provides a valuable natural plasma physics
502 laboratory.

503 **Acknowledgments**

504 We acknowledge NASA contract NAS5-02099 and V. Angelopoulos for use of data from
505 the THEMIS Mission. Specifically: O. LeContel and the late A. Roux for use of SCM
506 data, and K. H. Glassmeier, U. Auster and W. Baumjohann for the use of FGM data
507 provided under the lead of the Technical University of Braunschweig and with financial
508 support through the German Ministry for Economy and Technology and the German
509 Center for Aviation and Space (DLR) under contract 50 OC 0302. ARTEMIS data are
510 publicly available at <http://artemis.ssl.berkeley.edu>.

511 **References**

- 512 Angelopoulos, V. (2011, DEC). The ARTEMIS mission. *Space Science Reviews*,
513 *165*(1-4), 3-25. doi: 10.1007/s11214-010-9687-2
514 Auster, H. U., Glassmeier, K. H., Magnes, W., Aydogar, O., Baumjohann, W.,

- 515 Constantinescu, D., ... Wiedemann, M. (2008, DEC). The THEMIS
 516 Fluxgate Magnetometer. *Space Science Reviews*, 141(1-4), 235-264. doi:
 517 10.1007/s11214-008-9365-9
- 518 Burtis, W. J., & Helliwell, R. A. (1969). Banded chorus – A new type of VLF ra-
 519 diation observed in the magnetosphere by OGO 1 and OGO 3. *Journal of Geo-*
 520 *physical Research*, 74(11), 3002–3010. doi: 10.1029/JA074i011p03002
- 521 Burtis, W. J., & Helliwell, R. A. (1976). Magnetospheric chorus: Occurrence pat-
 522 terns and normalized frequency. *Planetary and Space Science*, 24(11), 1007–
 523 1024. doi: 10.1016/0032-0633(76)90119-7
- 524 Coroniti, F. V., Scarf, F. L., Kennel, C. F., Kurth, W. S., & Gurnett, D. A. (1980).
 525 Detection of Jovian whistler mode chorus; Implications for the Io torus aurora.
 526 *Geophysical Research Letters*, 7(1), 45–48. doi: 10.1029/GL007i001p00045
- 527 Cully, C. M., Angelopoulos, V., Auster, U., Bonnell, J., & Le Contel, O. (2011). Ob-
 528 servational evidence of the generation mechanism for rising-tone chorus. *Geo-*
 529 *physical Research Letters*, 38(1). doi: 10.1029/2010GL045793
- 530 Fu, X., Cowee, M. M., Friedel, R. H., Funsten, H. O., Gary, S. P., Hospodarsky,
 531 G. B., ... Winske, D. (2014). Whistler anisotropy instabilities as the source
 532 of banded chorus: Van allen probes observations and particle-in-cell simula-
 533 tions. *Journal of Geophysical Research: Space Physics*, 119(10), 8288-8298.
 534 Retrieved from [https://agupubs.onlinelibrary.wiley.com/doi/abs/](https://agupubs.onlinelibrary.wiley.com/doi/abs/10.1002/2014JA020364)
 535 [10.1002/2014JA020364](https://doi.org/10.1002/2014JA020364) doi: <https://doi.org/10.1002/2014JA020364>
- 536 Gao, X., Chen, L., Li, W., Lu, Q., & Wang, S. (2019). Statistical results of
 537 the power gap between lower-band and upper-band chorus waves. *Geo-*
 538 *physical Research Letters*, 46(8), 4098-4105. Retrieved from [https://](https://agupubs.onlinelibrary.wiley.com/doi/abs/10.1029/2019GL082140)
 539 agupubs.onlinelibrary.wiley.com/doi/abs/10.1029/2019GL082140 doi:
 540 <https://doi.org/10.1029/2019GL082140>
- 541 Gao, X., Lu, Q., Bortnik, J., Li, W., Chen, L., & Wang, S. (2016, MAR 28).
 542 Generation of multiband chorus by lower band cascade in the Earth's
 543 magnetosphere. *Geophysical Research Letters*, 43(6), 2343-2350. doi:
 544 10.1002/2016GL068313
- 545 Habagishi, T., Yagitani, S., & Omura, Y. (2014, JUN). Nonlinear damping of cho-
 546 rus emissions at local half cyclotron frequencies observed by GEOTAIL at L
 547 >9. *Journal of Geophysical Research: Space Physics*, 119(6), 4475-4483. doi:

548 10.1002/2013JA019696

549 Halekas, J. S., Delory, G. T., Lin, R. P., Stubbs, T. J., & Farrell, W. M. (2008,
550 SEP 4). Lunar prospector observations of the electrostatic potential of the

551 lunar surface and its response to incident currents. *Journal of Geophysical*
552 *Research-Space Physics*, *113*(A9). doi: 10.1029/2008JA013194

553 Halekas, J. S., Poppe, A., Delory, G. T., Farrell, W. M., & Horányi, M. (2012). Solar
554 wind electron interaction with the dayside lunar surface and crustal magnetic
555 fields: Evidence for precursor effects. *Earth, Planets and Space*, *64*(2), 3. doi:
556 10.5047/eps.2011.03.008

557 Halekas, J. S., Poppe, A. R., Farrell, W. M., Delory, G. T., Angelopoulos, V., Mc-
558 Fadden, J. P., ... others (2012). Lunar precursor effects in the solar wind and
559 terrestrial magnetosphere. *Journal of Geophysical Research: Space Physics*,
560 *117*(A5). doi: 10.1029/2011JA017289

561 Harada, Y., Andersson, L., Fowler, C. M., Mitchell, D. L., Halekas, J. S., Mazelle,
562 C., ... others (2016). MAVEN observations of electron-induced whistler mode
563 waves in the Martian magnetosphere. *Journal of Geophysical Research: Space*
564 *Physics*, *121*(10), 9717–9731. doi: 10.1002/2015GL067040

565 Harada, Y., & Halekas, J. S. (2016). Upstream waves and particles at the Moon.
566 In Keiling, A and Lee, DH and Nakariakov, V (Ed.), *Low-Frequency Waves in*
567 *Space Plasmas* (Vol. 216, p. 307-322).

568 Harada, Y., Halekas, J. S., Poppe, A. R., Kurita, S., & McFadden, J. P. (2014).
569 Extended lunar precursor regions: Electron-wave interaction. *Jour-*
570 *nal of Geophysical Research: Space Physics*, *119*(11), 9160–9173. doi:
571 10.1002/2014JA020618

572 Harada, Y., Halekas, J. S., Poppe, A. R., Tsugawa, Y., Kurita, S., & McFadden,
573 J. P. (2015, JUN). Statistical characterization of the forenoon particle and
574 wave morphology: ARTEMIS observations. *Journal of Geophysical Research:*
575 *Space Physics*, *120*(6), 4907-4921. doi: 10.1002/2015JA021211

576 Horne, R. B., Thorne, R. M., Shprits, Y. Y., Meredith, N. P., Glauert, S. A., Smith,
577 A. J., ... Decreau, P. M. E. (2005, SEP 8). Wave acceleration of elec-
578 trons in the Van Allen radiation belts. *Nature*, *437*(7056), 227-230. doi:
579 10.1038/nature03939

580 Hospodarsky, G. B., Averkamp, T. F., Kurth, W. S., Gurnett, D. A., Menietti,

- 581 J. D., Santolik, O., & Dougherty, M. K. (2008). Observations of chorus at Sat-
582 urn using the Cassini Radio and Plasma Wave Science instrument. *Journal of*
583 *Geophysical Research: Space Physics*, *113*(A12). doi: 10.1029/2008JA013237
- 584 Katoh, Y., & Omura, Y. (2011). Amplitude dependence of frequency sweep rates
585 of whistler mode chorus emissions. *Journal of Geophysical Research: Space*
586 *Physics*, *116*(A7). doi: 10.1029/2011JA016496
- 587 Kennel, C. F., & Petschek, H. E. (1966). Limit on stably trapped particle fluxes.
588 *Journal of Geophysical Research*, *71*(1), 1–28. doi: 10.1029/JZ071i001p00001
- 589 Khabibrakhmanov, I., & Summers, D. (1997, APR 1). On the theory of Alfvén
590 waves in the solar wind. *Journal of Geophysical Research: Space Physics*,
591 *102*(A4), 7095–7104. doi: 10.1029/96JA03843
- 592 Kurata, M., Tsunakawa, H., Saito, Y., Shibuya, H., Matsushima, M., & Shimizu,
593 H. (2005, DEC 28). Mini-magnetosphere over the Reiner Gamma magnetic
594 anomaly region on the Moon. *Geophysical Research Letters*, *32*(24). doi:
595 10.1029/2005GL024097
- 596 Kurita, S., Katoh, Y., Omura, Y., Angelopoulos, V., Cully, C. M., Le Contel, O., &
597 Misawa, H. (2012). THEMIS observation of chorus elements without a gap
598 at half the gyrofrequency. *Journal of Geophysical Research: Space Physics*,
599 *117*(A11). doi: 10.1029/2012JA018076
- 600 Menietti, J. D., Horne, R. B., Gurnett, D. A., Hospodarsky, G. B., Piker, C. W.,
601 & Groene, J. B. (2008). A survey of Galileo plasma wave instrument obser-
602 vations of Jovian whistler-mode chorus. *Annales Geophysicae*, *26*(7), 1819–
603 1828. Retrieved from <https://www.ann-geophys.net/26/1819/2008/> doi:
604 10.5194/angeo-26-1819-2008
- 605 Menietti, J. D., Santolik, O., Rymer, A. M., Hospodarsky, G. B., Gurnett, D. A., &
606 Coates, A. J. (2008). Analysis of plasma waves observed in the inner Saturn
607 magnetosphere. In *Annales Geophysicae: Atmospheres, Hydrospheres and*
608 *Space Sciences* (Vol. 26, p. 2631). doi: 10.1029/2007JA012856
- 609 Omura, Y. (2021, APR 20). Nonlinear wave growth theory of whistler-mode chorus
610 and hiss emissions in the magnetosphere. *Earth, Planets and Space*, *73*(1). doi:
611 10.1186/s40623-021-01380-w
- 612 Omura, Y., Hikishima, M., Katoh, Y., Summers, D., & Yagitani, S. (2009, JUL 18).
613 Nonlinear mechanisms of lower-band and upper-band VLF chorus emissions in

- 614 the magnetosphere. *Journal of Geophysical Research: Space Physics*, 114. doi:
615 10.1029/2009JA014206
- 616 Omura, Y., Katoh, Y., & Summers, D. (2008). Theory and simulation of the genera-
617 tion of whistler-mode chorus. *Journal of Geophysical Research: Space Physics*,
618 113(A4). doi: 10.1029/2007JA012622
- 619 Poppe, A. R., Farrell, W. M., & Halekas, J. S. (2018). Formation timescales of amor-
620 phous rims on lunar grains derived from artemis observations. *Journal of Geo-*
621 *physical Research: Planets*, 123(1), 37-46. Retrieved from [https://agupubs](https://agupubs.onlinelibrary.wiley.com/doi/abs/10.1002/2017JE005426)
622 [.onlinelibrary.wiley.com/doi/abs/10.1002/2017JE005426](https://agupubs.onlinelibrary.wiley.com/doi/abs/10.1002/2017JE005426) doi: 10.1002/
623 2017JE005426
- 624 Roux, A., Le Contel, O., Coillot, C., Bouabdellah, A., de la Porte, B., Alison, D.,
625 ... Vassal, M. C. (2008, DEC). The Search Coil Magnetometer for THEMIS.
626 *Space Science Reviews*, 141(1-4), 265-275. doi: 10.1007/s11214-008-9455-8
- 627 Sawaguchi, W., Harada, Y., & Kurita, S. (2021, JAN 16). Discrete rising tone
628 elements of whistler-mode waves in the vicinity of the Moon: ARTEMIS obser-
629 vations. *Geophysical Research Letters*, 48(1). doi: 10.1029/2020GL091100
- 630 Scarf, F. L., Gurnett, D. A., & Kurth, W. S. (1981). Measurements of plasma
631 wave spectra in Jupiter's magnetosphere. *Journal of Geophysical Re-*
632 *search: Space Physics*, 86(A10), 8181-8198. Retrieved from [https://](https://agupubs.onlinelibrary.wiley.com/doi/abs/10.1029/JA086iA10p08181)
633 agupubs.onlinelibrary.wiley.com/doi/abs/10.1029/JA086iA10p08181
634 doi: 10.1029/JA086iA10p08181
- 635 Shue, J. H., Chao, J. K., Fu, H. C., Russell, C. T., Song, P., Khurana, K. K., &
636 Singer, H. J. (1997, MAY 1). A new functional form to study the solar wind
637 control of the magnetopause size and shape. *Journal of Geophysical Research:*
638 *Space Physics*, 102(A5), 9497-9511. doi: 10.1029/97JA00196
- 639 Smith, E. J., & Tsurutani, B. T. (1976). Magnetosheath lion roars. *Jour-*
640 *nal of Geophysical Research: Space Physics*, 81(13), 2261-2266. doi:
641 10.1029/JA081i013p02261
- 642 Teng, S., Tao, X., & Li, W. (2019, APR 16). Typical characteristics of whistler
643 mode waves categorized by their spectral properties using Van Allen Probes
644 observations. *Geophysical Research Letters*, 46(7), 3607-3614. doi:
645 10.1029/2019GL082161
- 646 Thorne, R. M., Li, W., Ni, B., Ma, Q., Bortnik, J., Chen, L., ... Kanekal, S. G.

- 647 (2013, DEC 19). Rapid local acceleration of relativistic radiation-belt
648 electrons by magnetospheric chorus. *Nature*, 504(7480), 411+. doi:
649 10.1038/nature12889
- 650 Tsunakawa, H., Takahashi, F., Shimizu, H., Shibuya, H., & Matsushima, M. (2015,
651 JUN). Surface vector mapping of magnetic anomalies over the Moon using
652 Kaguya and Lunar Prospector observations. *Journal of Geophysical Research:
653 Planets*, 120(6), 1160-1185. doi: 10.1002/2014JE004785
- 654 Tsurutani, B. T., & Smith, E. J. (1974). Postmidnight chorus: A substorm phe-
655 nomenon. *Journal of Geophysical Research*, 79(1), 118-127. doi: 10.1029/
656 JA079i001p00118
- 657 Tsurutani, B. T., Smith, E. J., Anderson, R. R., Ogilvie, K. W., Scudder, J. D.,
658 Baker, D. N., & Bame, S. J. (1982). Lion roars and nonoscillatory drift mirror
659 waves in the magnetosheath. *Journal of Geophysical Research: Space Physics*,
660 87(NA8), 6060-6072. doi: 10.1029/JA087iA08p06060
- 661 Whipple, E. C. (1981). Potentials of surfaces in space. *Reports on Progress in
662 Physics*, 44(11), 1197-1250. doi: 10.1088/0034-4885/44/11/002